

A Numerical Simulation of Microphysical Structure of Cloud Associated with the 2008 Winter Freezing Rain over Southern China

Yang GAO

*Chinese Academy of Meteorological Sciences, China Meteorological Administration, Beijing, China
National Climate Center, China Meteorological Administration, Beijing, China*

Tongwen WU

National Climate Center, China Meteorological Administration, Beijing, China

Baode CHEN

Shanghai Typhoon Institute of China Meteorological Administration, Shanghai, China

Jun WANG

Department of Earth and Atmospheric Sciences, University of Nebraska -Lincoln, Lincoln, USA

and

Yiming LIU

National Climate Center, China Meteorological Administration, Beijing, China

(Manuscript received 2 July 2012, in final form 5 November 2012)

Abstract

The cloud microphysical structure for a freezing rain event between Jan 11 and Feb 4, 2008, over southern China is studied using the 30 km-mesh Weather Research and Forecasting (WRF) model simulations with four different microphysics schemes and CloudSat satellite observations. This 3-week-long freezing rain event, centered in the domain of 108°–113°E and 25°–28°N, has been extraordinarily rare over southern China during the recent 50 years. Except the Lin scheme, the other three microphysics schemes (Morrison, WSM6, and Thompson) yield WRF simulations that capture the temporal and spatial distribution of precipitation and surface air temperature associated with the freezing rain event, albeit the modeled center of precipitation is slightly drifted northward in comparison with the observation. The WRF simulations highlight the importance of the following characteristics of an atmospheric vertical thermal structure for forming freezing rain: above-freezing temperature in the middle troposphere (600–850 hPa) and below-freezing temperature in the lower troposphere (below 850 hPa). The temporal evolution of cloud structure and icing processing from Jan 11 to Feb 4 is also well simulated by WRF, which can be divided into two phases: (a) abundant liquid water is found below 700 hPa from Jan 20 to 26, 2008, and (b) liquid and solid water content coexist, and there are mixed-phase clouds in the whole column of atmosphere from Jan 26 to Feb 1, in particular, solid water dominated at the higher level, while liquid water dominated at the lower level. Such a change of cloud structure represents the typical ice-phase mechanism for the freezing rain such as on Jan 28, 2008, over the Hunan province.

Corresponding author: Tongwen Wu, National Climate Center, China Meteorological Administration, 46 Zhongguancun Nandajie, Beijing 100081, P. R. China.
E-mail: twwu@cma.gov.cn
©2013, Meteorological Society of Japan

Further evaluation with CloudSat observation over the Hunan province shows that the WRF model can capture the warm and refreezing layers near the surface, although it overestimates the solid water content.

Keywords freezing rain; WRF; CloudSat

1. Introduction

Extreme weather includes weather phenomena that are at the extremes of the historical distribution, especially severe or unseasonal weather (WMO, 2004). In recent decades, there has been a trend of increasing extreme weather events that are possibly linked to global warming (Fowler and Hennessy, 1995; Meehl et al. 2000; Easterling et al. 2000; Goswami et al. 2006; Wigley, 2009). In 2008, a widespread winter storm occurred across central, eastern, and mainly in southern China. This severe weather event persisted from Jan 11 to Feb 4, 2008. The duration and amount of precipitation have been extraordinarily rare during the recent 50 years (e.g., Shi et al. 2010). The timing of this event also coincided with the travel period during the Chinese Lunar New Year holidays, and hence, this event severely strained the country's transportation and energy networks, causing tens of thousands of travelers to be stranded at airports and train stations. In addition, the congestion on China's freight networks created a significant backlog of coal supplies that fuel a significant amount of the nation's power systems.

This severe weather event is characterized by rainfall freezing on the ground in a large area of southern China, and several studies have analyzed the causes of such an event (e.g., Ding et al. 2008; Wang et al. 2008a; Wen et al. 2009; Zhou et al. 2009; Sun and Zhao 2010; Gao et al. 2011). Wang et al. (2008a) and Wen et al. (2009) showed that the variability of the Arctic oscillation and the intensification of the southeastward Middle East jet stream were favorable for the occurrence of this event. Ding et al. (2008), Zhou et al. (2009), and Sun and Zhao (2010) indicated that the rapid development of a La Niña event and a persistent blocking high led to the intrusion of massive cold air into southern China. Wang et al. (2008b), Yang et al. (2008), and Shi et al. (2010) pointed out that the enhancement and northward shift of the subtropical western Pacific high (SWPH) and the eastward extension of the South Asian trough provided and maintained a sufficient supply of water vapor for the snow storm and freezing rain. Our previous diagnostic study (Gao et al. 2011) also showed that a persistent anomaly of an atmospheric thermodynamic structure was favorable for the formation of freezing rain in

association with the climatologically stronger south wind in the middle troposphere and stronger north wind in the lower troposphere.

Several studies about freezing rain events (Szeto et al. 1999; Rauber et al. 2000, 2001; Tremblay and Glazer 2000; Theriault 2010; Jeck 2011) have shown that the cloud microphysics structure plays an indispensable role in regulating the formation and evolution of snow or freezing rain. Freezing rain may be caused by two mechanisms: ice-phase mechanism and warm-rain mechanism. The latter does not need to have a warm layer (with temperature above 0°C) at the middle level of the clouds; in such cases, freezing rain is formed by a supercooled warm-rain process. The ice-phase mechanism or the classic process for freezing rain occurs when ice particles fall into the warm layer where the temperature exceeds 0°C, and subsequently, these particles go through a chain of processes from melting into liquid water in the warm layer, becoming supercool, and eventually freezing up on contact with the surface where the temperature is below 0°C. Which mechanism is more likely responsible for the 2008 winter freezing rain?

To better understand the cloud microphysical structure related to the extreme freezing rain event in 2008, we utilize the Weather Research and Forecasting (WRF) model together with the CloudSat satellite observation to explore the cloud microphysical structure during freezing events. In addition, it is also important to assess the sensitivity of the simulated results to the bulk microphysics schemes available in WRF, which not only has practical implications but also can provide useful information toward the improvement of cloud microphysics parameterization in the future.

The paper is divided as follows. In section 2, a brief description of the WRF simulation and data used is presented. In section 3, the simulation results are discussed. In section 4, the summary and conclusions are presented.

2. Model and data used

The model used in this study is the Advanced Research WRF (ARW) version 3.1.1 (Skamarock et al. 2008). The WRF model is commonly used for mesoscale numerical weather prediction and simula-

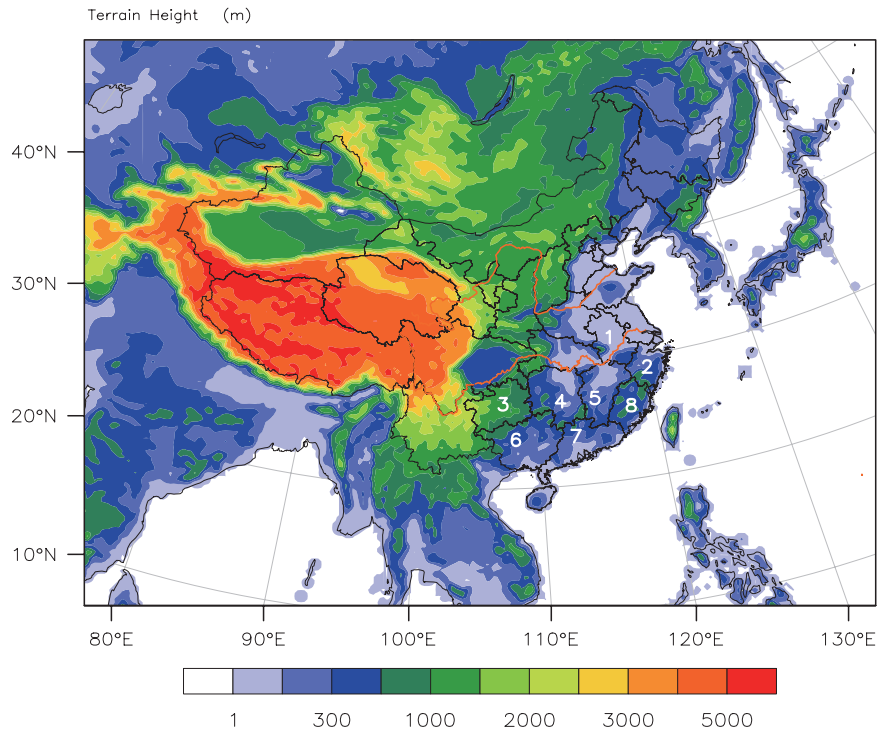


Fig. 1. Model domain and topographic height (m) with a grid spacing of 30 km. Numbers in white denote some provinces (1: Anhui, 2: Zhejiang, 3: Guizhou, 4: Hunan, 5: Jiangxi, 6: Guangxi, 7: Guangdong, 8: Fujian).

tion (e.g., Davis et al. 2008; Xu et al. 2009; Clark et al. 2010; Ward and Cotton 2011). Recently, it has also been used as a regional climate model for studying the influence of atmospheric rivers and land surface conditions on heavy rain and flooding, seasonal precipitation in the U.S. (Leung and Qian 2009; Bukovsky and Karoly 2009), the regional climate in Europe and polar regions (Argüeso et al. 2011; Cassano et al. 2011), and the East Asian summer monsoon in 1998 (Kim and Wang 2011).

The model domain is centered at 34°N and 105°E, covers the whole Tibetan Plateau and the majority of the area of East Asia (Fig. 1), and consists of 232 × 181 grid points in the zonal and meridional directions. The horizontal grid spacing is 30 km. The model physics schemes are selected as follows: the Kain-Fritsch cumulus convection scheme (Kain and Fritsch 1990, 1993; Kain 2004), the Community Atmosphere Model (CAM) radiation scheme, the Noah land surface model (Chen and Dudhia 2001; Sertel et al. 2009; Zhang et al. 2009), the Yonsei University planetary boundary layer scheme, and the gravity wave drag parameterization (Hong et al. 2008). Initial and boundary conditions for the simulation are derived

from the NCEP Reanalysis 2 (Kanamitsu et al. 2002). The simulation is initialized at 12:00 UTC, November 1, 2007; thus, there is a long-term period to gradually create a more reasonable land surface condition to match the atmospheric state before the freezing event and performed till the end of February 2008 with lateral boundary data updated every six hours. Time-varying sea surface temperature is also updated with the same time interval.

Four WRF simulations are carried out, and the only difference in their configuration is the cloud microphysics scheme that varies in sequence from the following schemes: the Morrison 2-moment scheme (Morrison and Pinto 2006; Morrison et al. 2005, 2009), Purdue Lin scheme (single moment) (Chen and Sun 2002), WSM 6-class graupel scheme (single moment) (Hong and Lim 2006), and Thompson graupel scheme (2-moment scheme in V3.1) (Thompson et al. 2004). All four schemes partition condensed water into cloud water, rain water, cloud ice, snow, and graupel.

Three observation data sets are used: (1) daily precipitation and surface temperature data collected at 640 ground stations in China, which are provided by the National Meteorological Information Center,

China Meteorological Administration; (2) global $2.5^\circ \times 2.5^\circ$ gridded daily atmospheric temperatures from the National Center for Atmospheric Research (NCEP-NCAR) reanalysis (Kalnay et al. 1996); and (3) two CloudSat standard data of the level 2B Radar-only Cloud Water Content (2B-CWC-RO) product (algorithm version 5.1), Geometrical profile product (2B-GEOPROF) and Cloudsat ECMWF-AUX Auxiliary Data publicly available from <http://cloudsat.cira.colostate.edu/>. CloudSat is the second satellite in the "A Train" satellite constellation (Stephens et al. 2002). The 94-GHz cloud profiling radar (CPR) on the satellite can provide global-scale cross sections of the cloud vertical structure (e.g., Matrosov et al. 2008; Hamada and Nishi 2010; Protat et al. 2011). Each CloudSat orbit takes 98.7 minutes with 14.56 orbits per day. There are approximately 36,383 profiles per orbit, and each profile has 125 vertical bins for a total vertical window of 30 km. Unfortunately, CloudSat did not provide valid estimates of the cloud liquid water due to the solution diverges on the selected orbits in this study. In fact, the liquid water content from 2B-CWC-RO is always missing. However, the partition algorithm in 2B-CWC-RO is separately applied to the ice and liquid phases regardless of whether both retrievals were successful. In other words, if the liquid retrieval fails to converge, the ice water will still be scaled such that it goes to zero as the temperature increases to 0°C . Therefore, the ice water contents from 2B-CWC-RO are available for analysis in this study. In addition, the vertical profiles of the CPR radar reflectivity factor are from the 2B-GEOPROF product while the temperature is from the ECMWF-AUX product.

3. Results

3.1 Simulation of freezing rain

This extreme event began on 11 Jan and ended on Feb 4, 2008. Figure 2 shows the spatial distribution of total precipitation accumulated between Jan 11 and Feb 4, 2008. The ground-based observations (Fig. 2a) show a belt of strong precipitation that starts from the southwest of Guangxi and Guangdong provinces and spreads northeastward to the Jiangxi and Fujian provinces where the maximum reaches more than 125 mm. All the simulations of different microphysics schemes well reproduce the precipitation belt in southern China, and the spatial pattern of precipitation closely resembles the observations, although the simulated precipitation amount differs from the observed amount in various regions. Comparatively, the Morrison scheme gives a better result for the spatial

pattern and amount of precipitation (Fig. 2b).

However, the core areas that suffered the disaster of freezing rain in winter 2008 are not located in the strong precipitation belt discussed above; instead, they are in the northwestern side of this belt, i.e., in the Hunan and Guizhou provinces where both the ground (Fig. 2a) and simulation (Fig. 2b) observations show only 75–125 mm precipitation during the period.

When rain falls from the sky onto the ground, the surface air temperature is an important meteorological factor to determine its freezing. Figure 3 shows the daily mean temperature averaged from Jan 11 to Feb 4, 2008, from the in-site observations and the WRF simulation. The surface air temperature is commonly found in the range from -1°C to -4°C , which is favorable for rain freezing near the ground surface, and explains that the Hunan and Guizhou provinces (Fig. 3a) are the core regions of freezing rain. To the southeast of this low-temperature region and in the belt of the largest amount of precipitation belt shown in Fig. 2, the surface air temperature is above freezing, and thus, freezing rain does not occur there. There are large variations of the simulated temperature associated with freezing rain. The WSM6 and Thompson schemes, and in particular, the Morrison scheme can simulate the low-temperature anomaly over the Hunan and Guizhou provinces (Fig. 3b). Comparatively, Figs. 3d and 3e show that the simulated temperature over the core region of disaster is slightly lower than the observation (Fig. 3a). However, the simulation with the Lin scheme can hardly represent this anomaly phenomenon.

Since the inner core region of freezing rain disaster is centered at the domain of $108^\circ\text{--}113^\circ\text{E}$ and $25^\circ\text{--}28^\circ\text{N}$ (Figs. 2 and 3), our following analysis will focus on this domain. Figure 4 shows the time-latitude cross section of precipitation averaged for $108^\circ\text{--}113^\circ\text{E}$, indicating the three episodes of precipitation that occurred in the inner core region (about $25^\circ\text{--}28^\circ\text{N}$) between Jan 11 and 15, Jan 16 and 22, and Jan 23 and Feb 3, respectively. The main area of precipitation during the first episodes is located between 26°N and 38°N , and the maximum of precipitation reaches about $5\text{--}10 \text{ mm day}^{-1}$. This rain belt then moves southward to 22°N during the second episode and further spreads southward to 18°N in the third episode. Among all three episodes, the third episode has the longest duration (11 days) of continuous precipitation, with reported maximum rainfall exceeding 20 mm day^{-1} in the $24^\circ\text{N}\text{--}26^\circ\text{N}$ zone. The timeline of this continuous rainfall in southern China is also well simulated by WRF regardless of which microphysics scheme is used;

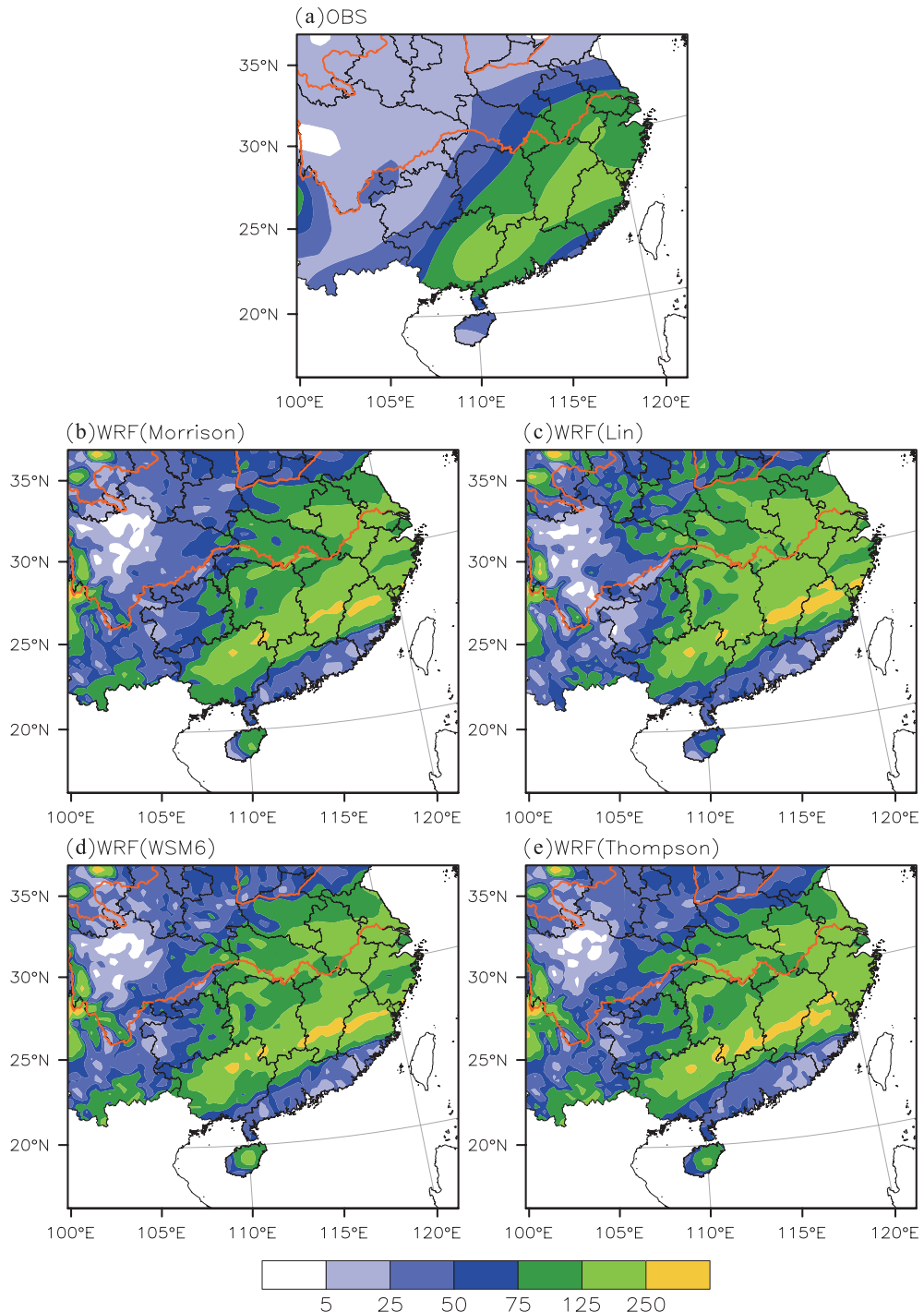


Fig. 2. Spatial distribution of total precipitation (mm) accumulated from Jan 11 to Feb 4, 2008, for rain gauge observation and WRF simulation with four different microphysics schemes. (a) OBS, (b) Morrison, (c) Lin, (d) WSM6, (e) Thompson. The Yangtze and Yellow Rivers are drawn as brown lines. The OBS is the observation.

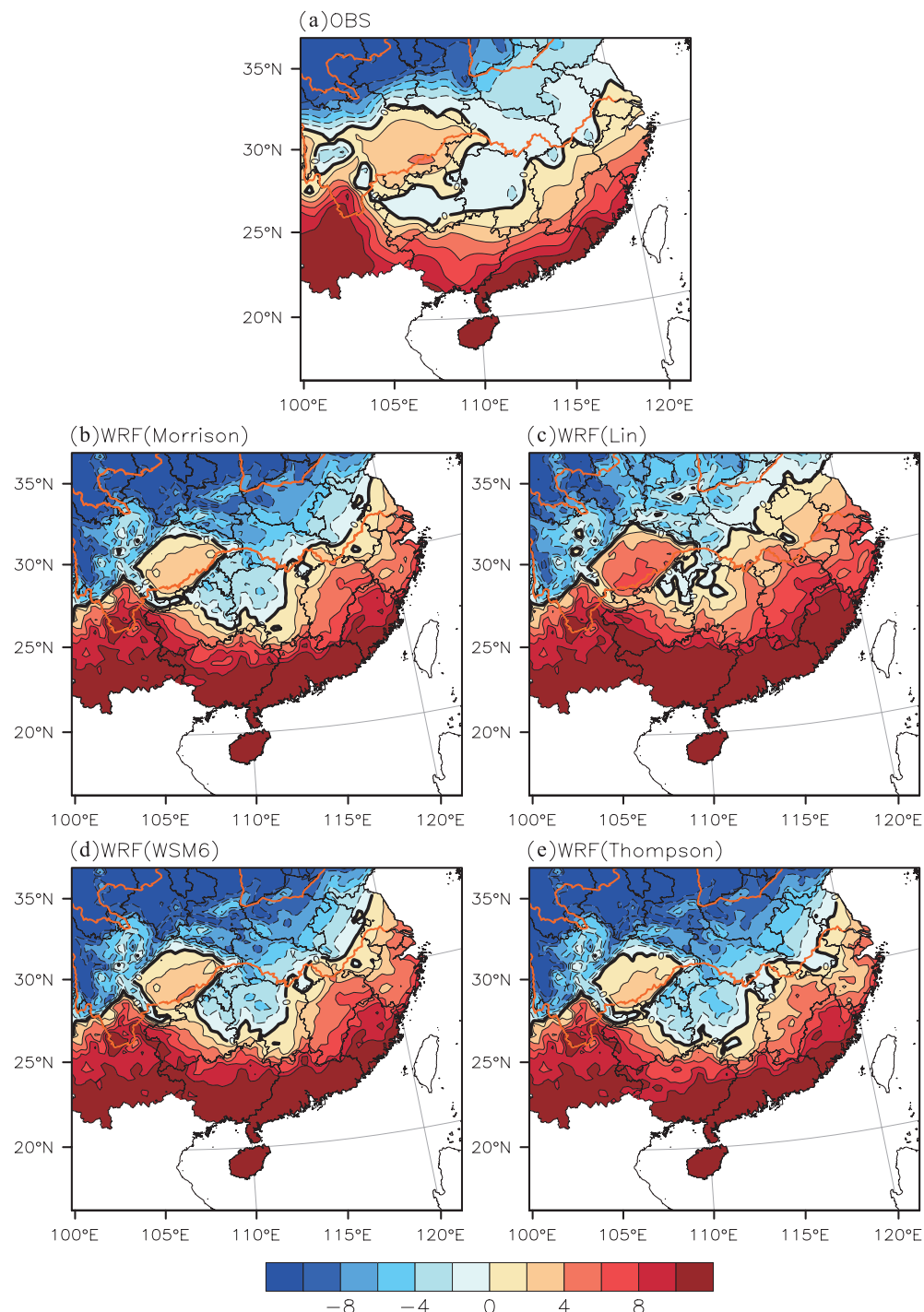


Fig. 3. Mean daily temperature ($^{\circ}\text{C}$) averaged from Jan 11 to Feb 4, 2008, for surface observation and WRF simulation. (a) OBS, (b) Morrison, (c) Lin, (d) WSM6, (e) Thompson. The interval of contour lines is 2°C .

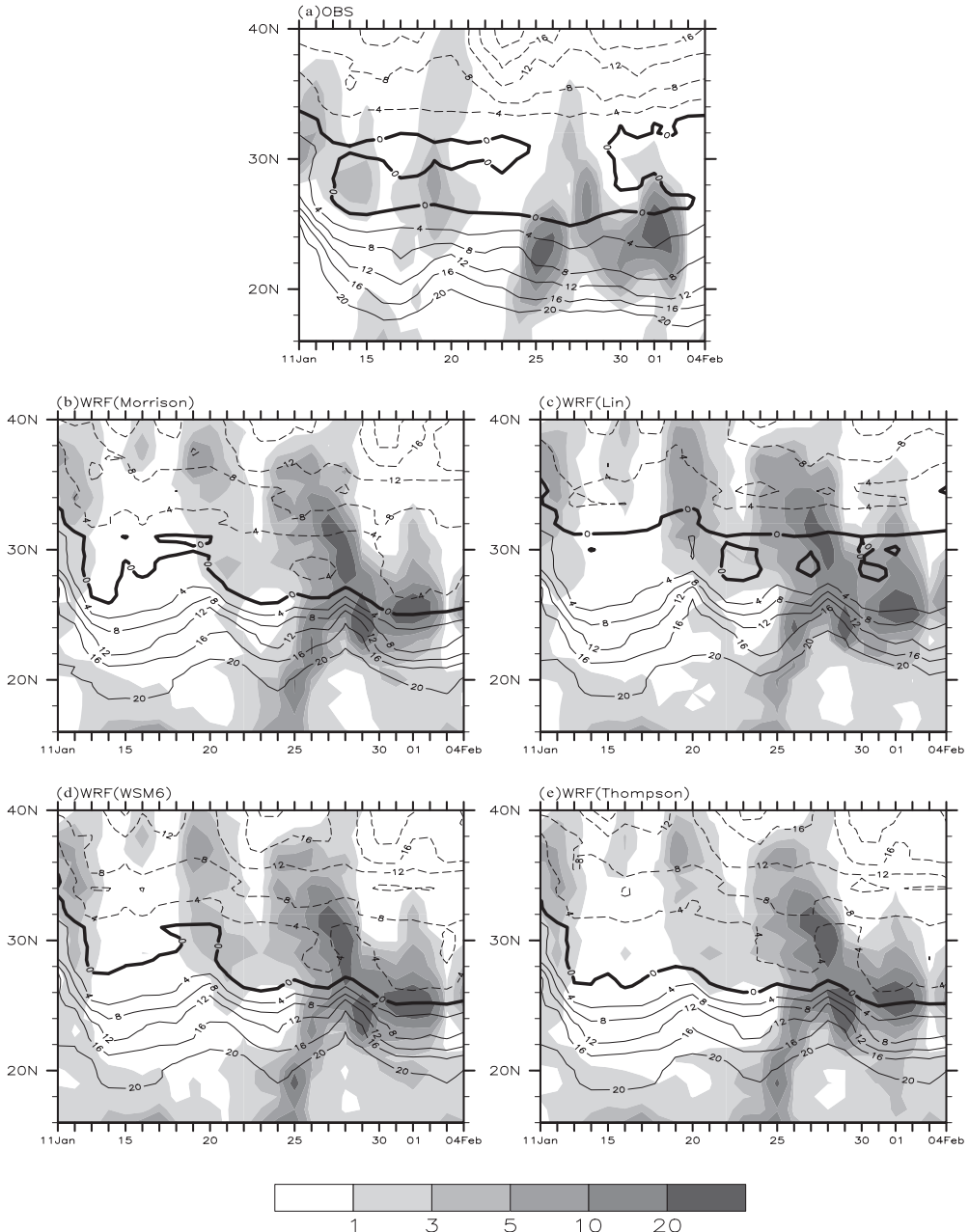


Fig. 4. Time-latitude cross section of mean daily precipitation along 16° – 40° N (units: mm day^{-1} , shaded area) and air surface temperature (units: $^{\circ}\text{C}$, contour line) averaged for 108° – 113° E from Jan 11 to Feb 4, 2008, for observation and WRF simulation with four different microphysics schemes. (a) OBS, (b) Morrison, (c) Lin, (d) WSM6, (e) Thompson.

however, all simulations produce too much precipitation between 30° N and 40° N, and the maximum of precipitation exceeds 20 mm day^{-1} . In Figs. 4b, 4d, and 4e, all of the WRF simulations show a clear band of the surface air temperature lower than 0°C between 26° N and 30° N from Jan 20 to Feb 3, which is the exact

location of freezing rain. Similar to the finding in Fig. 3c, the surface air temperature simulated by the Lin scheme is higher compared with observation.

3.2 Vertical thermal structure

The thermodynamic structure of the atmosphere is

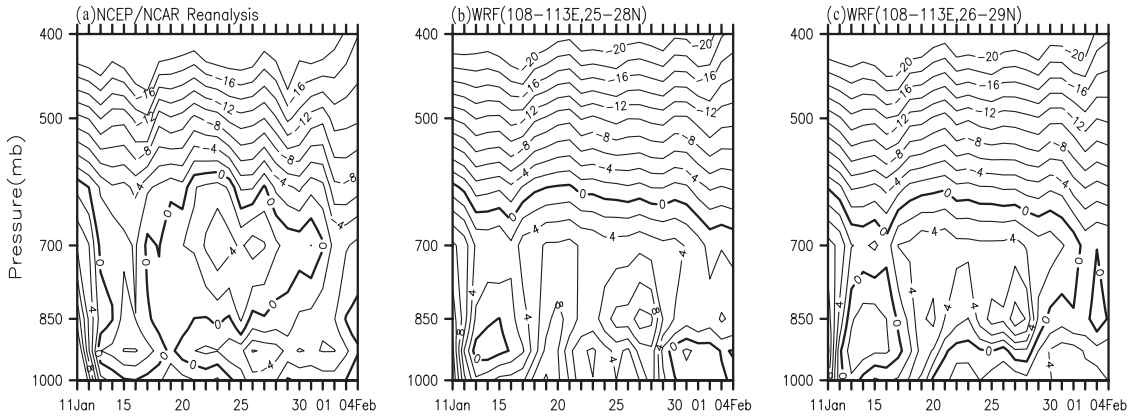


Fig. 5. Altitude-time section of mean atmospheric temperature ($^{\circ}\text{C}$) from Jan 11 to Feb 4, 2008, for (a) NCEP/NCAR reanalysis (averaged for 108°E – 113°E and 25°N – 28°N), (b) WRF simulation with the Morrison scheme (averaged for 108°E – 113°E and 25°N – 28°N), (c) WRF simulation with the Morrison scheme (averaged for 108° – 113°E and 26° – 29°N).

essential for freezing rain as the precipitation must be in the form of rainfall, not snowfall, before it reaches the ground. Figure 5a shows the altitude-time section of daily mean atmospheric temperature below 400 hPa from Jan 11 to Feb 4, 2008, averaged for the region of 108° – 113°E and 25° – 28°N from the NCEP reanalysis data. It features that cold (lower than 0°C) air above 600 hPa, warm air of 0 – 4°C in the 850–600 hPa layer, and cold air of -2°C to -4°C below 850 hPa from Jan 19 to Feb 1. This vertical structure of temperature is propitious for the formation of ice or snow at altitudes higher than 600 hPa, in the melting layer at 650–850 hPa as a result of ice-water droplet coalescence, snow thawing or ice melting when falling from a higher altitude to the middle troposphere, and freezing after mid-tropospheric liquid water droplets fall on the ground.

As shown in Figs. 2 and 3, the WRF model with the Morrison scheme can give better results for the simulation of precipitation and air temperature. Therefore, we further analyze the WRF simulation with this scheme. As shown in Fig. 5b, the Morrison scheme considerably captures the characteristics of colder temperature (less than 0°C) above \sim 600 hPa and warmer temperature below in the 108° – 113°E and 25° – 28°N domain, although the WRF model fails to reproduce a layer colder than 0°C below 850 hPa from Jan 19 to Feb 1 in the same region. The model-simulated near surface air (in Fig. 5b) is warmer than the counterpart of the NCEP reanalysis data (in Fig. 5a). In contrast, if we move the analyzed area 1° northward to 108° – 113°E and 26° – 29°N (Fig. 5c), the simulated structure is much more similar to the

observed vertical structure of temperature, as shown in Fig. 5a.

3.3 Vertical structure of cloud microphysics

In WRF, the mixing ratio of cloud water (Qcloud), rainwater (Qrain), cloud ice (Qice), snow (Qsnow), and graupel (Qgraup) are prognostic variables. Qcloud and Qrain denote the amount of liquid water in the form of cloud droplets and rain droplets, respectively. Qsnow, Qice, Qgraup are the indicators of amount of water in the form of snow, ice, and graupel in the atmosphere, respectively. Figure 6 illustrates the altitude-time section of those model-simulated variables of the Morrison scheme from Jan 11 to Feb 4, averaged for 108° – 113°E and 26° – 29°N . During the persistent episode with 3 – 5 mm day^{-1} rainfall in the latitude band of 26° – 30°N (Fig. 4), a large amount of cloud water and rain water below 700 hPa from Jan 20 to 26, 2008, is found, but no solid water content (such as snow, ice, or graupel) exists (Fig. 6a and 6b). From Jan 26 to Feb 1, the cloud water spreads from the lower troposphere up to 400 hPa. In addition, ice and snow exist above the 600 hPa level, and the rain water increases below 600 hPa. The total rain in WRF is the sum of precipitation from the cumulus scheme (RAINC) and the microphysics scheme (RAINNC). As shown in Fig. 6f, the RAINNC takes the most of rainfall from Jan 11 to Feb 4, and there is some rainfall owing to the active convective activity from Jan 26 to 30. In other words, the precipitation in this freezing event is mostly nonconvective from Jan 11 to Feb 4, largely due to the long-time confront between cold and warm air in southern China (Gao et al. 2011).

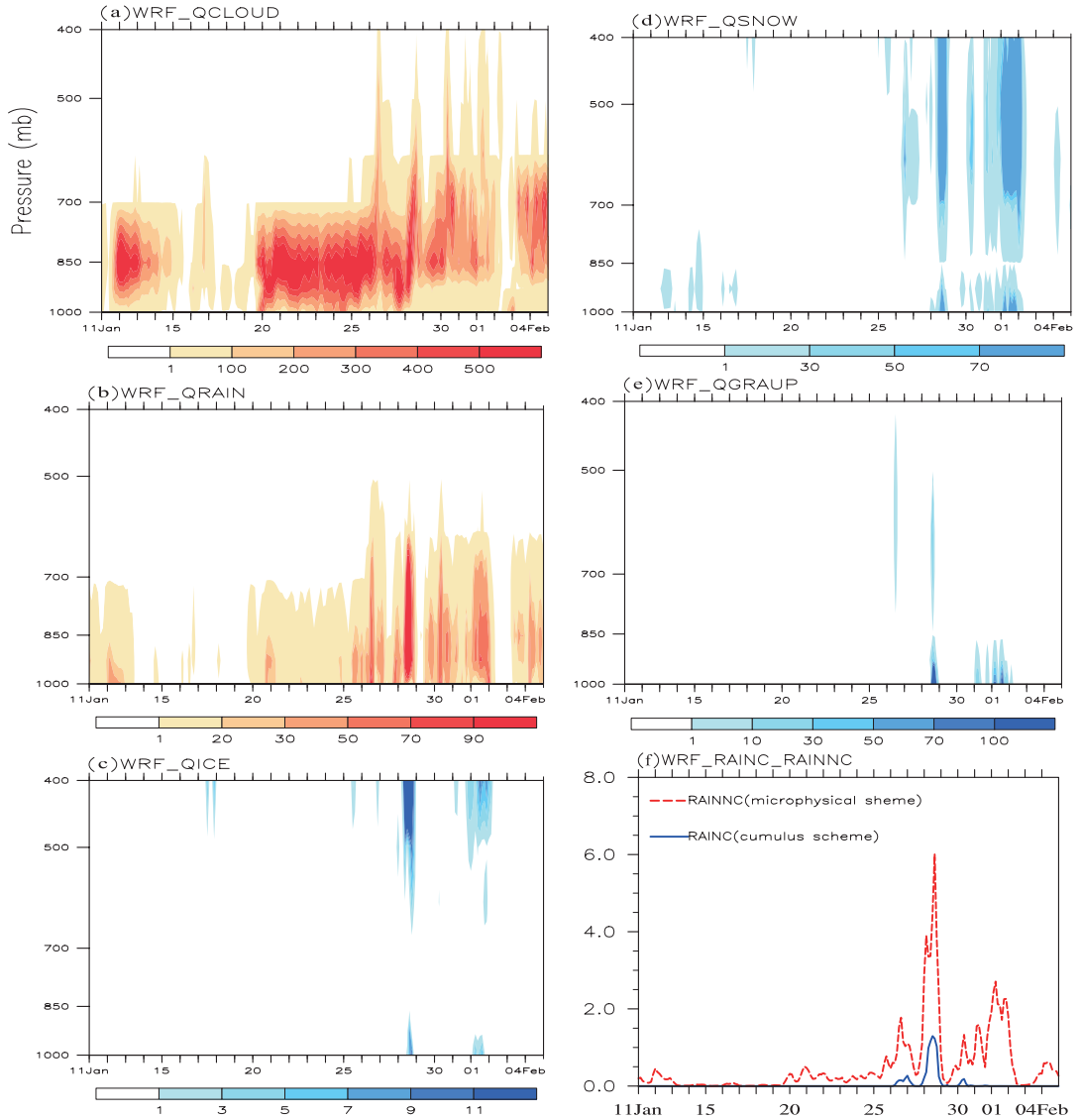


Fig. 6. Altitude-time section of WRF simulation with the Morrison scheme averaged for 108° – 113° E and 26° – 29° N from Jan 11 to Feb 4, 2008, for the mass content of (a) cloud water (b) rain water (c) ice (d) snow (e) graupel, and (f) every three hours of precipitation of WRF simulation averaged for the same area. RAINC (blue line) comes from the cumulus scheme, and the RAINNC (red line) comes from the microphysics scheme. The units are in mg m^{-3} in (a) to (e) and in mm in (f).

Figure 7 shows the liquid fraction of surface precipitation and air surface temperature every three hours simulated by the four different microphysics schemes. There are no large variations of rainfall simulated by these four microphysics schemes. Except the Lin scheme, others show similar variations of the air surface temperature. Quantitatively, the simulated daily precipitation is less than the observation in the first two episodes of Jan 11–15 and Jan 16–22 (Fig. 8a),

while all the microphysics schemes simulate more rain from Jan 23 to Feb 3. As the observed temperature vibrates around the 0°C on Jan 14 to Feb 4, the amount of precipitation occurring when the surface temperature is less 0°C can be regarded as potential freezing rain amount. Except the Lin scheme, the other schemes (Morrison, WSM6, and Thompson) can basically capture this phenomenon from Jan 22 to 31.

As shown in Fig. 6f, the maximum of rain amount

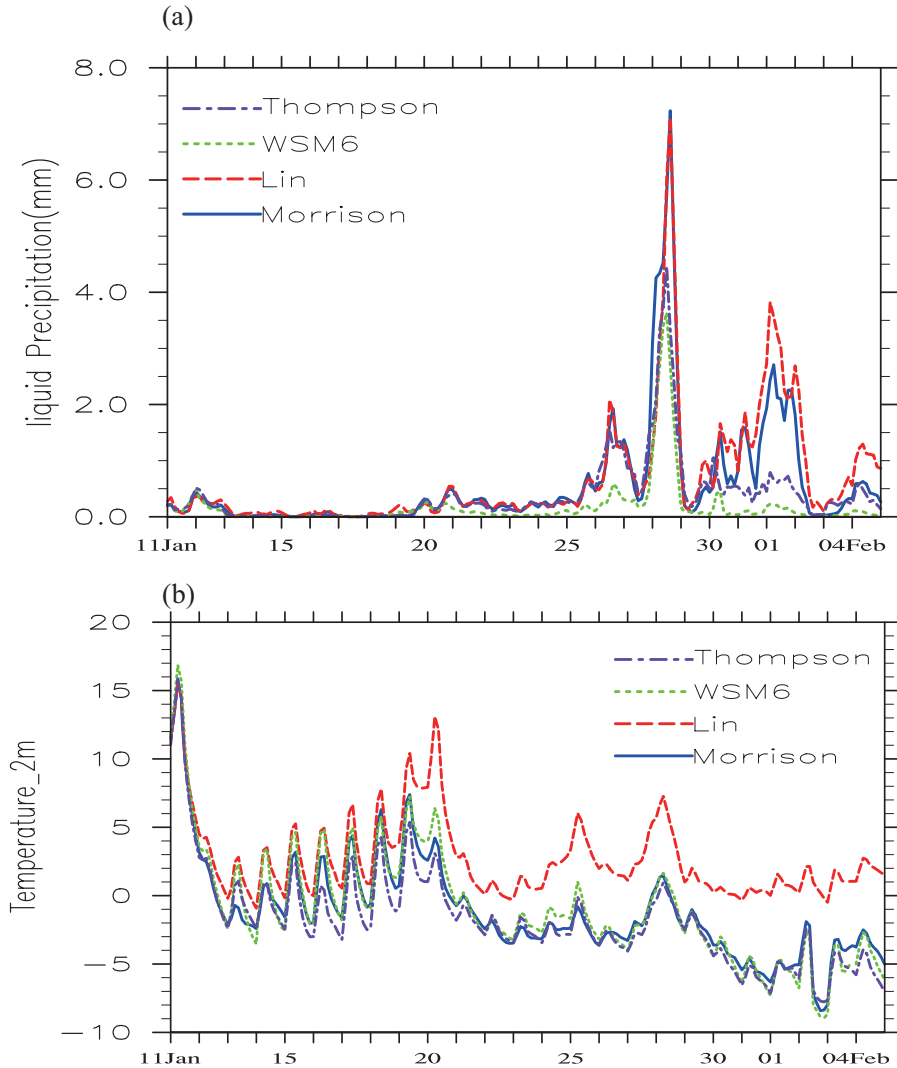


Fig. 7. (a) Liquid fraction of surface precipitation (mm (3 h)^{-1}) and (b) air surface temperature ($^{\circ}\text{C}$) simulated by the four different microphysics schemes averaged for $108^{\circ}\text{--}113^{\circ}\text{E}$ and $26^{\circ}\text{--}29^{\circ}\text{N}$ from Jan 11 to Feb 4, 2008. The Morrison, Lin, WSM6, and Thompson schemes are shown by a blue solid line, red line, green line, and purple line, respectively.

occurs on Jan 28. The vertical profile of condensate content (Qcloud, Qrain, Qice, Qsnow, and Qgraup) on Jan 28 averaged for the region of $108^{\circ}\text{--}113^{\circ}\text{E}$ and $26^{\circ}\text{--}29^{\circ}\text{N}$ is helpful for further understanding the cloud structure for freezing rain. As shown in Fig. 9, there are large differences in the vertical profile of hydrometeors in the four microphysics schemes. The largest difference is noticed for the simulation of solid content. Compared to the other schemes, the Lin scheme simulates small ice-phase particles, a smaller depth of clouds, a higher temperature at the cloud top at the middle level of the clouds. Therefore, in the

simulation by the Lin scheme, the increase of the cloud water and rain water amount belongs to the vapor deposition process. The warm-rain process is dominant, and the temperature near the surface is above 0°C in the Lin scheme, both of which are not beneficial for the development of freezing rain. Comparatively, the temperature simulated by other microphysics schemes is similar, with a common feature of a warm layer in the middle level, and the temperature below 0°C near the surface. As shown in Figs. 9a, 9c, and 9d, the amount of snow simulated by the Morrison, WSM6, and Thompson schemes is greater above 600 hPa and

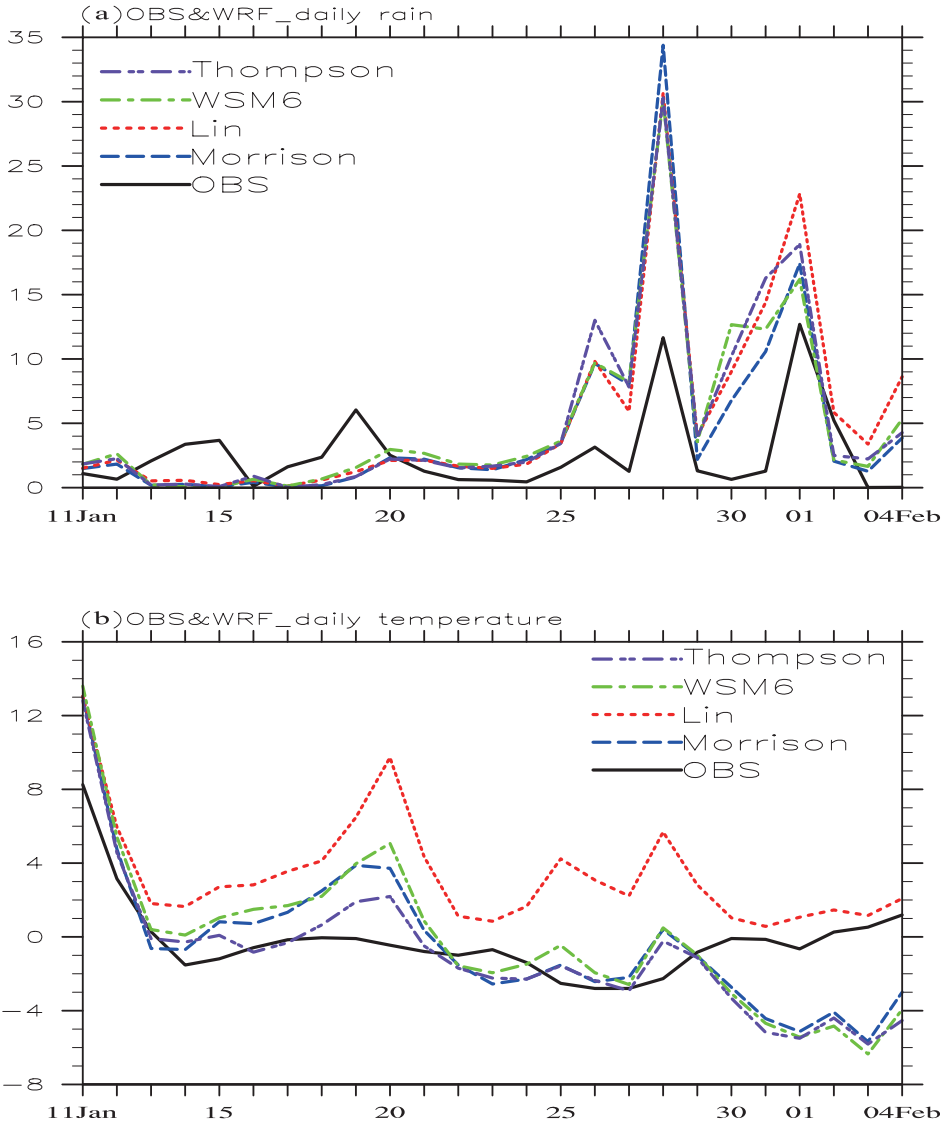


Fig. 8. (a) Daily precipitation (mm) and (b) air surface temperature ($^{\circ}$ C) averaged for 108 $^{\circ}$ –113 $^{\circ}$ E and 26 $^{\circ}$ –29 $^{\circ}$ N from Jan 11 to Feb 4, 2008, for observation and WRF simulation with four different microphysics schemes. The OBS, Morrison, Lin, WSM6, and Thompson schemes are shown by a black solid line, blue line, red line, green line, purple line, respectively.

decreases rapidly to zero in the lower and warm layers with the temperature above 0 $^{\circ}$ C. The observation indicates that snow and ice are completely melted in the deeply warm layer. In Fig. 9, there are large amounts of cloud water and rain water between 640 hPa and 940 hPa. Except the melting of solid particles at the high level, they are mainly attributed to the strong horizontal transport of water vapor, as shown in the right panels of Figs. 9a–9d. In other words, the warm-rain process dominated between 640 hPa and

940 hPa. The simulations by three microphysics schemes (Morrison, WSM6, Thompson) also consistently show that the temperature is lower than 0 $^{\circ}$ C below 940 hPa and is presumably related to the cold air from North China (Gao et al. 2011). Hence, snow crystals, graupel, cloud water, and rain water all coexist in this layer. Comparatively, the WSM6 scheme simulates more ice and graupel at the high level than others.

In this freezing event, Figs. 9a, 9c, and 9d exactly

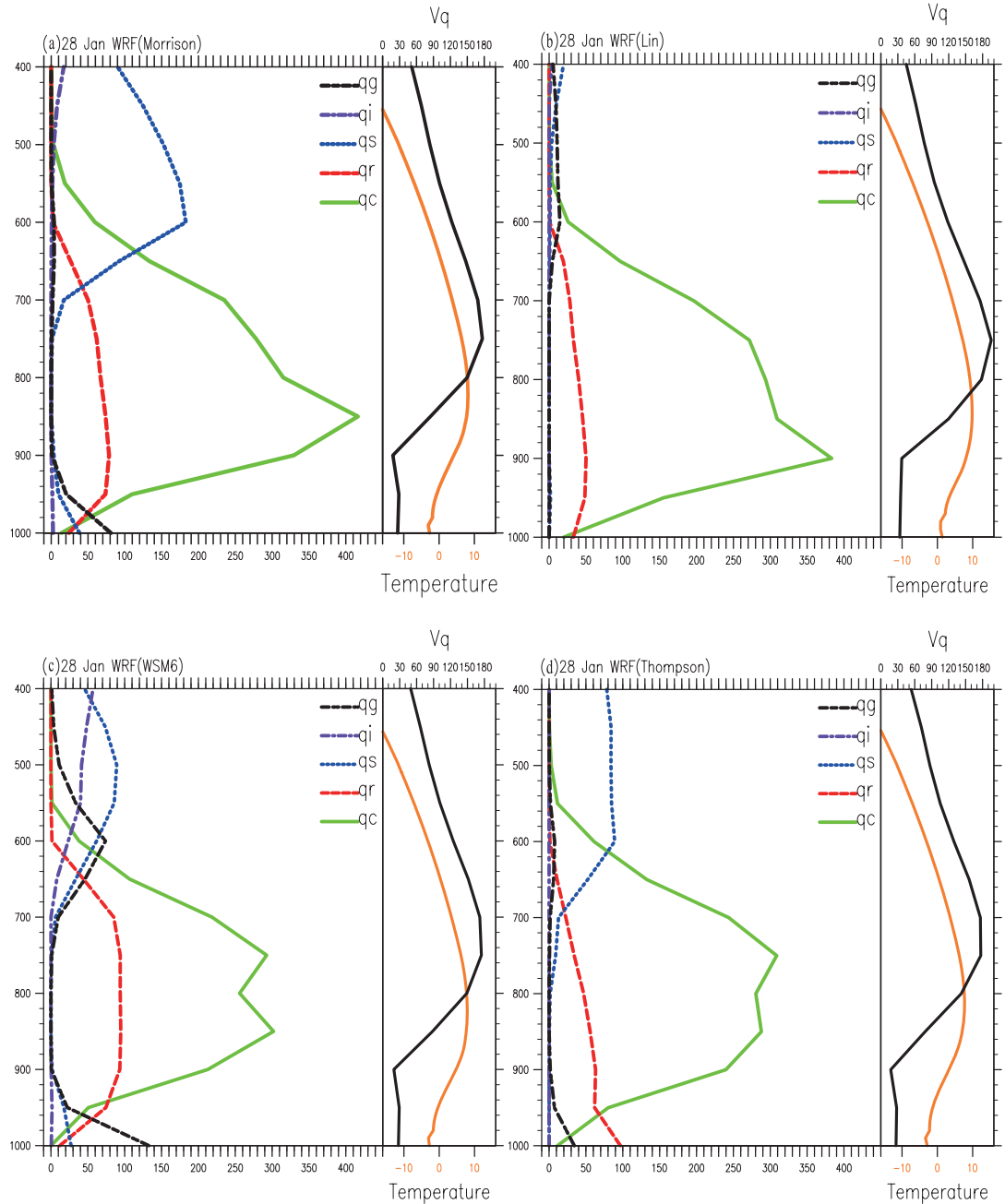


Fig. 9. Vertical profiles of condensate content (mg m^{-3}), atmospheric temperature ($^{\circ}\text{C}$), and horizontal water vapor transport ($\text{g m kg}^{-1} \text{s}^{-1}$) from WRF simulation with four different microphysics schemes on Jan 28, averaged for 108° – 113°E and 26° – 29°N . Cloud water (qc) is shown by a green solid line, rain water (qr) as a red line, snow (qs) as a blue line, ice (qi) as a purple line, graupel (qg) as a black dash line, temperature as a brown solid line, horizontal water vapor transport (Vq) as a black solid line (a) Morrison, (b) Lin, (c) WSM6, and (d) Thompson.

show a typical ice-phase mechanism in which large amounts of solid particles (snow and ice) at the high level fall into a middle-level warm layer to form

supercooled drops that in turn instantly freeze when they strike the ground that has a refreezing layer. The snow and ice particles at the lower level (below 940

hPa) are in favor of the persistence of the snow and freezing weather. Although the location of the inversion layer in the WRF simulation has a northward bias as compared with the NCEP reanalysis (Fig. 5), the model captures the mechanism for this freezing rain over 108° – 113° E and 26° – 29° N in the Hunan province on Jan 28.

CloudSat observations can provide an evaluation of cloud microphysics. From Jan 11 to Feb 4, CloudSat passed over the region of freezing rain in South China six times: the orbit 9085 on Jan 12, 9107 on Jan 13, 9311 on Jan 27, 9318 on Jan 28, 9369 on Jan 31, and 9376 on Feb 1. Because of continuous rainfall in late January, the Hunan province (shown in Fig. 1) is the worst disaster-struck area by freezing rain, and the orbits 9318 and 9369 are selected for the following analysis as they exactly pass over this province.

Figure 10a shows the path of orbit 9318 of CloudSat from 05: 53 to 05: 57 UTC, Jan 28, 2008; this track passes from point A (114.43° E, 20.00° N) to point B (111.45° N, 31.99° N). As illustrated in Fig. 10b, the instantaneous cross section of radar reflectivity indicates a deep cloud layer from 2 to 8 km over 27° – 29° N. From Fig. 10c, most of the hydrometeors in the Morrison scheme can be found at an altitude of 1–9 km over 26° – 32° N with the maximum value of 500 mg m^{-3} , same is true for an altitude of 4–8 km over 25° – 26.5° N. Therefore, the simulated cloud fraction is drifted northward from CloudSat. As shown in Fig. 10d, at an altitude of 2–4 km over 26.5° – 28.5° N, the radar reflectivity values are high, but are devoid of ice water content, indicating prevailing liquid water droplets. In other words, there is a warm layer with the temperature above 0°C . Moreover, some ice water content exists at an altitude of 2–5 km near point B. A comparison with the simulated temperature and ice content (sum of cloud ice, snow, and graupel) by the Morrison scheme shows that the modeled vertical structure of the water phase is quite similar to the observation, albeit the model tends to simulate a larger ice water content than the 2B-CWC-RO product (Fig. 10e).

In addition, another orbit of 9369 also crosses from point C (113.05° E, 31.99° N) to point D (110.07° E, 20.00° N) over the Hunan province within from 18: 31 to 18: 35 UTC, Jan 31, 2008 (Fig. 11a). As shown in Figs. 11b and 11c, the position and thickness of the cloud from the Morrison scheme are simulated reasonably well. Most of the ice water content is located at an altitude of 4–9 km over 24° – 30° N, and another center of the ice water content exists in the lower atmosphere over 26° – 32° N (Fig. 11d). A warm

layer at an altitude of 2–4 km over 25° – 28° N is also distinct. The simulation by the Morrison scheme captures all the features described by CloudSat. The model captures the ice structure over 25° – 27° N, but not the observed ice water content over 28° – 30° N (Fig. 11e).

4. Conclusions

The WRF simulation for a significant freezing rain event over southern China is studied, with an emphasis on the examination of the sensitivity of the simulation to the selection of the microphysics schemes including Morrison, Lin, WSM6, and Thompson. In comparison to the ground-based weather report, NCEP re-analysis data, and CloudSat data, the WRF model simulations with four different microphysics schemes can all reproduce the distinct rain belt averaged from Jan 11 to Feb 4 in southern China and remarkable continuous rainfall from Jan 23 to Feb 3.

Except the Lin scheme, all other three microphysics schemes can yield simulation results that are consistent with the characteristics of observed abnormal low surface temperature. The inner core region of freezing rain in the region of 108° – 113° E and 25° – 28° N are also simulated and in good agreement with observations. Among the four schemes, the Morrison scheme results show a relatively better agreement with the observed rainfall and air surface temperature. In addition, the simulated vertical structure of temperature that accounts for the formation of freezing rain is also well simulated by the WRF model with this scheme, although the simulated location is drifted slightly northward. In addition, except the Lin scheme, others can reproduce the daily surface temperature below 0°C when the surface precipitation occurred from Jan 22 to 31. Overall, the Morrison, WSM6, and Thompson schemes can produce a typical ice-phase mechanism for the formation of freezing rain, while the Lin scheme shows the warm-rain mechanism. In the main period of freezing rain, ice cloud particles fall from above 600 hPa into a middle-level warm layer, and the resulting rain droplets forms frozen rain when they strike the ground with a surface temperature lower than 0°C . A comparison with the two orbits of CloudSat data such as on Jan 28 and 31, 2008, shows that WRF captures the locations of the warm layer (liquid water layer) and refreezing layer in the atmosphere.

We also noticed the following model biases: (a) the rain belt has a slight shift northward for this freezing rain event, and (b) the simulated ice water content tends to be larger than the estimate by CloudSat. While our analysis is limited to a particular event, and hence is

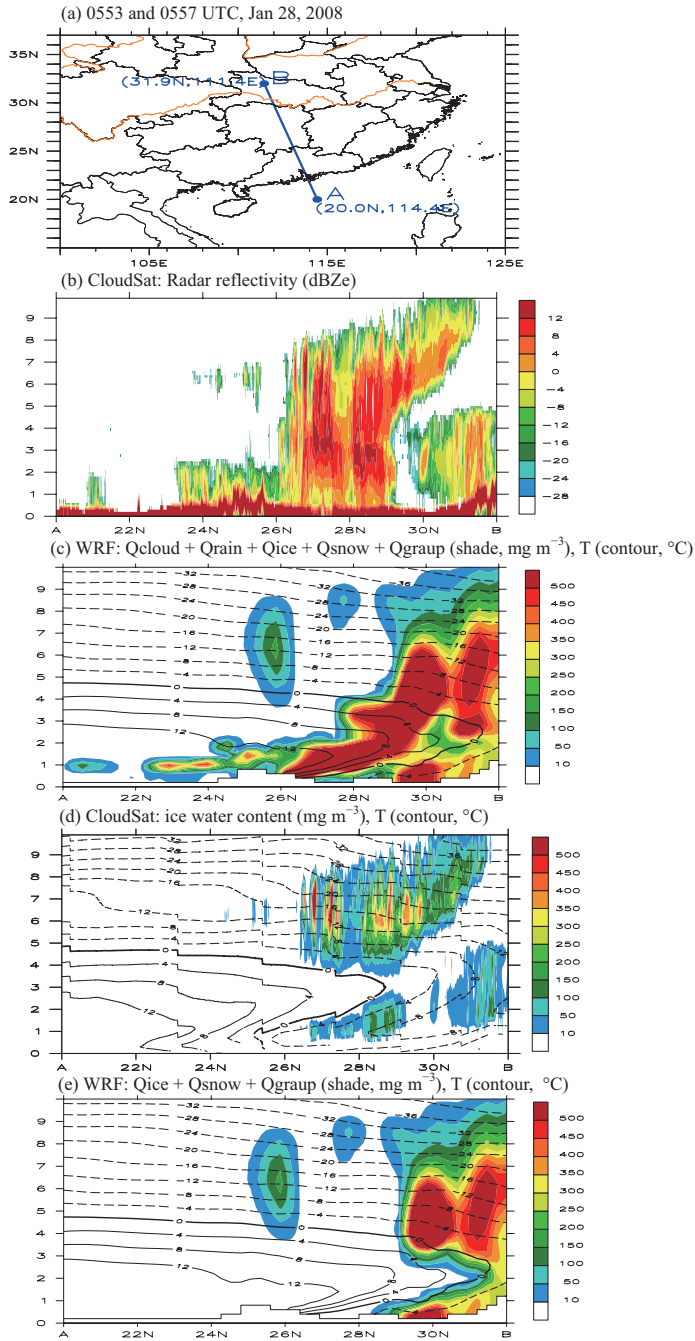


Fig. 10. (a) Path of the 9318 orbit of CloudSat from 05: 53 to 05: 57 UTC, Jan 28, 2008, (b) Cross section of CloudSat-observed radar reflectivity (Unit: dBZe) from point A (114.43°E, 20.00°N) to point B (111.45°N, 31.99°N), (c) The corresponding WRF-simulated temperature (°C, contour line) with the Morrison scheme and the sum of cloud water, rain water, cloud ice, snow, and graupel amount (mg m^{-3} , shaded area) at 0600 UTC, Jan 28, 2008, (d) Cross section of CloudSat-observed ice water content (mg m^{-3}) and temperature (°C, contour line) from point A to point B, and (e) Corresponding WRF-simulated temperature (°C, contour line) with the Morrison scheme and the sum of cloud ice, snow, and graupel amount (mg m^{-3} , shaded area).

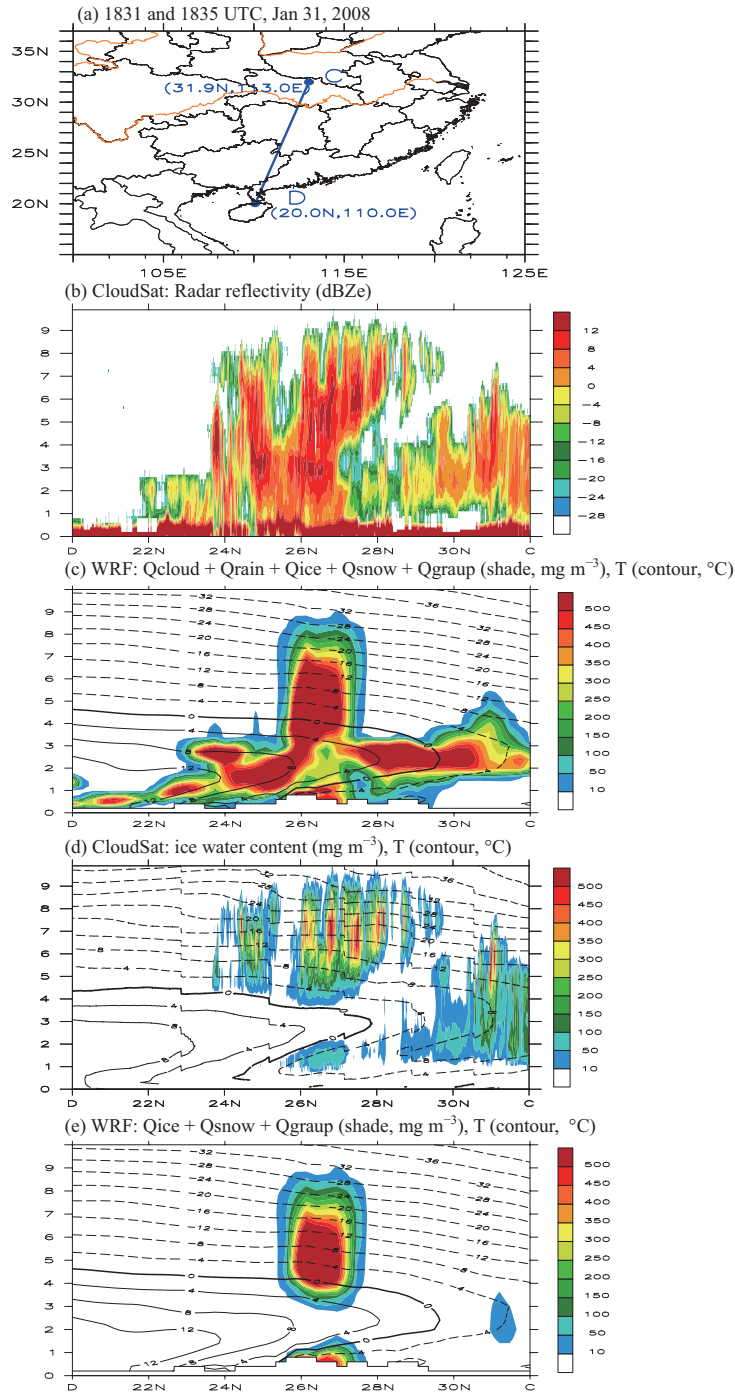


Fig. 11. The same as Figure 10, but from point C ($113.05^{\circ}\text{E}, 31.99^{\circ}\text{N}$) to point D ($110.07^{\circ}\text{E}, 20.00^{\circ}\text{N}$) from 18:31 to 18:35 UTC, Jan 31, 2008.

not able to study if these biases are systematic in nature, the results of this study indicate that a long-term analysis of cloud microphysics in China through

WRF simulations and the analysis of CloudSat data is warranted. Since the liquid water content from CloudSat is always missing, a combined use of

CloudSat-based information of the ice water content, temperature, and radar reflectivity together with model simulations is needed to identify freezing rain events.

Acknowledgments

This work was supported by the National Basic Research Program of China (973 Program: 2010CB951902) and the Special Program for China Meteorology Trade (Grant No. GYHY200806006).

References

- Argüeso, D., J. M. Hidalgo-Muñoz, S. R. Gámiz-Fortis, M. J. Esteban-Parra, J. Dudhia, and Y. Castro-Díez, 2011: Evaluation of WRF parameterizations for climate studies over southern Spain using a multistep regionalization. *J. Climate*, **24**, 5633–5651.
- Bukovsky, M. S., and D. J. Karoly, 2009: Precipitation simulations using WRF as a nested regional climate model. *J. Appl. Meteor. Climatol.*, **48**, 2152–2159.
- Cassano, J. J., M. E. Higgins, and M. W. Seefeldt, 2011: Performance of the weather research and forecasting model for month-long pan-arctic simulations. *Mon. Wea. Rev.*, **139**, 3469–3488.
- Chen, F., and J. Dudhia, 2001: Coupling an advanced land-surface hydrology model with the Penn State-NCAR MM5 modeling system. PartI: Model description and implementation. *Mon. Wea. Rev.*, **129**, 569–585.
- Chen, S. H., and W. Y. Sun, 2002: A one-dimensional time dependent cloud model. *J. Meteor. Soc. Japan*, **80**, 99–118.
- Clark, A. J., W. A. Gallus, and M. L. Weisman, 2010: Neighborhood-based verification of precipitation forecasts from convection-allowing ncar wrf model simulations and the operational nam. *Wea. Forecasting*, **25**, 1495–1509.
- Davis, C. A., W. Wang, S. Chen, Y. Chen, K. Corbosiero, M. DeMaria, J. Dudhia, G. Holland, J. Klemp, J. Michalakes, H. Reeves, R. Rotunno, and Q. Xiao, 2008: Prediction of landfalling hurricanes with the advanced hurricane wrf model. *Mon. Wea. Rev.*, **136**, 1990–2005.
- Ding, Y. H., Z. Y. Wang, Y. F. Song, and J. Zhang, 2008: Causes of the unprecedented freezing disaster in January 2008 and its possible association with the global warming. *Acta Meteorologica Sinica*, **66**, 808–825 (in Chinese).
- Easterling, D. R., J. L. Evans, P. Y. Groisman, T. R. Karl, K. E. Kunkel, and P. Ambenje, 2000: Observed variability and trends in extreme climate events: a brief review. *Bull. Amer. Meteor. Soc.*, **81**, 417–425.
- Fowler, A. M., and K. J. Hennessy, 1995: Potential impacts of global warming on the frequency and magnitude of heavy precipitation. *Natural Hazards*, **11**, 283–303.
- Gao, Y., T. W. Wu, and B. D. Chen, 2011: Anomalous thermodynamic conditions for freezing rain in southern China in January 2008 and their causes. *Plateau Meteorology*, **30**, 1526–1533 (in Chinese).
- Goswami, B. N., V. Venugopal, D. Sengupta, M. S. Madhusoodanan, and P. K. Xavier, 2006: Increasing trend of extreme rain events over India in a warming environment. *Science*, **314**, 1442–1444.
- Hamada, A., and N. Nishi, 2010: Development of a cloud-top height estimation method by geostationary satellite split-window measurements trained with cloudsat data. *J. Appl. Meteor. Climatol.*, **49**, 2035–2049.
- Hong, S. Y., and J. O. J. Lim, 2006: The WRF Single-Moment 6-class microphysics scheme (WSM6). *J. Korean Meteor. Soc.*, **42**, 129–151.
- Hong, S. Y., J. Choi, E. C. Chang, H. Park, and Y. J. Kim, 2008: Lower-tropospheric enhancement of gravity wave drag in a global spectral atmospheric forecast model. *Wea. Forecasting*, **23**, 523–531.
- Jeck, R. K., 2011: Spatial and microphysical characteristics of low-ceiling, temperature-inverted clouds in warm overrunning and freezing-rain conditions: a case study. *J. Appl. Meteor. Climatol.*, **50**, 2062–2072.
- Kain, J. S., and J. M. Fritsch, 1990: A one-dimensional entraining/detraining plume model and its application in convective parameterization. *J. Atmos. Sci.*, **47**, 2784–2802.
- Kain, J. S., and J. M. Fritsch, 1993: Convective parameterization for mesoscale models: The Kain-Fritsch scheme. *The representation of cumulus in mesoscale models*. Meteorological Monographs, No. 46, Amer. Meteor. Soc., 165–170.
- Kain, J. S. 2004: The Kain-Fritsch convective parameterization: An update. *J. Appl. Meteor.*, **43**, 170–181.
- Kalnay, E., and co-authors, 1996: The NCEP/NCAR 40-Year Reanalysis Project. *Bull. Amer. Meteor. Soc.*, **77**, 437–471.
- Kanamitsu, M., W. Ebisuzaki, J. Woollen, S-K Yang, J. J. Hnilo, M. Fiorino, and G. L. Potter, 2002: NCEP-DOE AMIP-II Reanalysis (R-2). *Bull. Amer. Meteor. Soc.*, **83**, 1631–1643.
- Kim, H., and B. Wang, 2011: Sensitivity of the WRF model simulation of the East Asian summer monsoon in 1993 to shortwave radiation schemes and ozone absorption. *Asia-Pacific Journal of Atmospheric Sciences*, **47**, 167–180.
- Leung, L. R., and Y. Qian, 2009: Atmospheric rivers induced heavy precipitation and flooding in the western U.S. simulated by the WRF regional climate model. *Geophys. Res. Lett.*, **36**, L03820.
- Matrosov, S. Y., A. Battaglia, and P. Rodriguez, 2008: Effects of multiple scattering on attenuation-based retrievals of stratiform rainfall from cloudsat. *J. Atmos. Oceanic Technol.*, **25**, 2199–2208.
- Meehl, G. A., F. Zwiers, J. Evans, T. Knutson, L. Mearns, and P. Whetton, 2000: Trends in extreme weather and climate events: issues related to modeling extremes in projections of future climate change. *Bull. Amer. Meteor. Soc.*, **81**, 427–436.

- Morrison, H., J. A. Curry, and V. I. Khvorostyanov, 2005: A new double-moment microphysics parameterization for application in cloud and climate models, PartI: Description. *J. Atmos. Sci.*, **62**, 1665–1677.
- Morrison, H., and J. O. Pinto, 2006: Intercomparison of bulk microphysics schemes in mesoscale simulations of springtime Arctic mixed-phase stratiform clouds. *Mon. Wea. Rev.*, **134**, 1880–1900.
- Morrison, H., G. Thompson, and V. Tatarskii, 2009: Impact of cloud microphysics on the development of trailing stratiform precipitation in a simulated squall line: comparison of one- and two-moment schemes. *Mon. Wea. Rev.*, **137**, 991–1007.
- Protat, A., D. Bouniol, E. J. O'Connor, H. K. Baltink, J. Verlinde, and K. Widener, 2011: CloudSat as a global radar calibrator. *J. Atmos. Oceanic Technol.*, **28**, 445–452.
- Rauber, R. M., L. S. Olthoff, M. K. Ramamurthy, and K. E. Kunkel, 2000: The relative importance of warm rain and melting processes in freezing precipitation events. *J. Appl. Meteor.*, **39**, 1185–1195.
- Rauber, R. M., L. S. Olthoff, M. K. Ramamurthy, and D. Miller, 2001: A synoptic weather pattern and sounding-based climatology of freezing precipitation in the United States east of the Rocky Mountains. *J. Appl. Meteor.*, **39**, 1185–1195.
- Sertel, E., A. Robock, and C. Ormeci, 2009: Impacts of land cover data quality on regional climate simulations. *Int. J. Climatol.*, **30**, 1942–1953.
- Shi, X. H., X. D. Xu, and C. G. Lu, 2010: The dynamic and thermodynamic structures associated with a series of heavy precipitation events over china during January 2008. *Wea. Forecasting.*, **25**, 1124–1141.
- Skamarock, W. C., J. B. Klemp, J. Dudhia, D. O. Gill, D. M. Barker, W. Wang, and J. G. Powers, 2008: *A description of the advanced research WRF version 3*. NCAR technical note, NCAR/TN-475 + STR, 125pp.
- Stephens, G. L., and Coauthors, 2002: The CloudSat mission and the a-train. *Bull. Amer. Meteor. Soc.*, **83**, 1771–1790.
- Sun, J. H., and S. X. Zhao, 2010: The impacts of multiscale weather systems on freezing rain and snowstorms over southern china. *Wea. Forecasting.*, **25**, 388–407.
- Szeto, K. K., A. Tremblay, H. Guan, D. R. Hudak, R. E. Stewart, and Z. Cao, 1999: The mesoscale dynamics of freezing rain storms over eastern Canada. *J. Atmos. Sci.*, **56**, 1261–1281.
- Theriault, J. M., R. E. Stewart, and W. Henson, 2010: On the dependence of winter precipitation types on temperature, precipitation rate, and associated features. *J. Appl. Meteor. Climatol.*, **49**, 1429–1442.
- Thompson, G., R. M. Rasmussen, and K. Manning, 2004: Explicit forecasts of winter precipitation using an improved bulk microphysics scheme. PartI: Description and sensitivity analysis. *Mon. Wea. Rev.*, **132**, 519–542.
- Tremblay, A., and A. Glazer, 2000: An improved modeling scheme for freezing precipitation forecasts. *Mon. Wea. Rev.*, **128**, 1289–1308.
- Wang, Y. F, Y. Li, P. Y. Li, and Y. Liu, 2008a: The large scale circulation of the snow disaster in south China in the beginning of 2008. *Acta Meteorologica Sinica*, **66**, 826–835 (in Chinese).
- Wang, D. H., and Coauthors, 2008b: A preliminary analysis of features and causes of the snow storm event over the Southern China in January 2008. *Acta Meteorologica Sinica*, **66**, 405–422 (in Chinese).
- Ward, D., and W. Cotton, 2011: A method for forecasting cloud condensation nuclei using predictions of aerosol physical and chemical properties from WRF/Chem. *J. Appl. Meteor. Climatol.*, **50**, 1601–1615.
- Wen, M., S. Yang, A. Kumar, and P. Q. Zhang, 2009: An analysis of the large-scale climate anomalies associated with the snowstorms affecting china in January 2008. *Mon. Wea. Rev.*, **137**, 1111–1131.
- Wigley, T. M. L., 2009: The effect of changing climate on the frequency of absolute extreme events. *Climatic Change.*, **97**, 67–76.
- Xu, J., S. Rugg, L. Byerle, and Z. Liu, 2009: Weather forecasts by the wrf-arw model with the gsi data assimilation system in the complex terrain areas of southwest asia. *Wea. Forecasting.*, **24**, 987–1008.
- Yang, G. M., Q. Kong, D. Y. Mao, F. H. Zhang, Z. M. Kang, and Z. P. Zong, 2008: Analysis of the long-lasting cryogenic freezing rain and snow weather in the beginning of 2008. *Acta Meteorologica Sinica*, **66**, 836–849 (in Chinese).
- Zhang, Y. X., V. Duliére, P. W. Mote, and E. P. Salathé, 2009: Evaluation of wrf and hadrm mesoscale climate simulations over the U.S. pacific northwest. *J. Climate.*, **22**, 5511–5526.
- Zhou, W., J. C. L. Chan, W. Chen, J. Ling, J. G. Pinto, and Y. P. Shao, 2009: Synoptic-scale controls of persistent low temperature and icy weather over southern china in January 2008. *Mon. Wea. Rev.*, **137**, 3978–3991.
- World Meteorological Organization (WMO), 2004: Workshop on Severe and Extreme Events Forecasting. Toulouse, 25pp.